

THE TIMING BEHAVIOR OF THE CENTRAL COMPACT OBJECT PULSAR 1E 1207.4–5209

E. V. GOTTHELF AND J. P. HALPERN

Columbia Astrophysics Laboratory, Columbia University, New York, NY 10027-6601, USA; eric@astro.columbia.edu

ABSTRACT

We present 20 years of timing observations for 1E 1207.4–5209, the central compact object in supernova remnant PKS 1209–51/52, to follow up on our detection of an unexpected timing glitch in its spin-down. Using new *XMM-Newton* and *NICER* observations of 1E 1207.4–5209, we now find that the phase ephemeris can be well-modelled by either two small glitches, or extreme timing noise. The implied magnitudes of the frequency glitches are $\Delta f/f = (9 \pm 2) \times 10^{-10}$ and $\Delta f/f = (3.7 \pm 0.7) \times 10^{-10}$, at epochs 2010.9 and 2014.4, respectively. The updated timing solutions also rule out our previous suggestion of a large glitch in the frequency derivative \dot{f} . No other canonical pulsar with such a small spin-down rate ($\dot{f} = -1.2 \times 10^{-16}$ Hz s⁻¹) or surface dipole magnetic field strength ($B_s = 9.8 \times 10^{10}$ G) has been observed to glitch; the glitch activity parameter of 1E 1207.4–5209 is larger than that of more energetic pulsars. Alternative parameterizations that do not involve glitches can fit the data, but they have timing residuals or a second frequency derivative \ddot{f} that are orders of magnitude larger than in pulsars with similar spin-down parameters. These timing properties of 1E 1207.4–5209 further motivate the leading theory of central compact objects, that an initial B -field of normal strength was buried in the neutron star crust by fallback of supernova ejecta, suppressing the surface dipole field. The slow reemergence of the buried field may be involved in triggering glitches or excess timing noise. *Subject headings:* pulsars: individual (1E 1207.4–5209, PSR J1210–5226) — stars: neutron

1. INTRODUCTION

The central compact object (CCO) 1E 1207.4–5209 in the supernova remnant (SNR) PKS 1209–51/52 has been studied intensively because of its unusual timing and spectral properties. It was the first CCO pulsar discovered (Zavlin et al. 2000), the first isolated neutron star (NS) to display strong absorption lines in its X-ray spectrum (Sanwal et al. 2002; Mereghetti et al. 2002; Bignami et al. 2003; De Luca et al. 2004), and most recently, the first CCO to show glitch activity (Gotthelf & Halpern 2018). 1E 1207.4–5209 is one of the three known CCO pulsars, all with characteristic weak surface dipole magnetic field strength, (2.9, 3.1, and 9.8) $\times 10^{10}$ G, the smallest known among young pulsars (Gotthelf & Halpern 2007; Gotthelf et al. 2013; Halpern & Gotthelf 2010, 2011, 2015).

CCOs are young NSs associated with SNRs defined by their steady surface thermal X-ray emission, lack of surrounding pulsar wind nebula, and nondetection at any other wavelength (Pavlov et al. 2002; see De Luca et al. 2017 for a recent review). CCOs are as numerous as other classes of NS in SNRs, implying that they represent a significant fraction of NS births. In addition to the three CCO pulsars, ~ 7 NSs with similar properties have eluded searches for pulsations. They may have even weaker magnetic fields, more uniform surface temperature distribution, or an unfavorable viewing geometry.

The spin-down magnetic field inferred for 1E 1207.4–5209, $B_s = 9.8 \times 10^{10}$ G, is remarkably close to $B \approx 8 \times 10^{10}$ G, the value measured from its spectroscopic absorption features, interpreted as the electron cyclotron fundamental at 0.7 keV and its harmonics. This agreement has all but eliminated competing ideas for the origin of the absorption lines, and provides a convincing confirmation of the surface B -field strength.

The recent discovery of a glitch from 1E 1207.4–5209 (Gotthelf & Halpern 2018) is most unexpected given the absence of glitches in pulsars with such small \dot{f} and B_s . Possibly related is the problem of how hot spots are created on the NS surface, as evidenced by the X-ray pulse modulation, in the absence of a strong magnetic field. Halpern & Gotthelf (2010) reviewed theoretical arguments for CCOs having magnetar strength internal toroidal fields $\sim 10^{14}$ G, possibly buried during the formation of the NS, that could account for their hot spots and high X-ray luminosity without contributing to their weak external dipole fields. Ho (2015) hypothesized that glitch activity in CCOs may be triggered by such strong magnetic fields diffusing through the NS crust and interacting with the neutron superfluid there.

We present *Chandra*, *XMM-Newton* and *NICER* observations of 1E 1207.4–5209 that confirm the original detection of a glitch and reveal a second glitch, and a possibly third, that suggest a recurrence time of 4–10 years. In Section 2, we describe the new X-ray timing observations. In Section 3, we present the updated timing solutions that rule out a large glitch in the frequency derivative as previously reported. We also explore alternative timing models for the pulsar rotation that can be interpreted as timing noise. Section 4 compares the results with the general pulsar population, and Section 5 concludes with implications for the origin of glitches, timing noise, and CCOs themselves.

2. DATA ANALYSIS

We have obtained new timing observations of 1E 1207.4–5209 using the *NICER* and *XMM-Newton* observatories that allow us to resolve ambiguities in the glitch analysis reported in Gotthelf & Halpern (2018) and to consider alternative interpretations. We supplement archival *NICER* data sets starting from 2017 July

24 with our subsequent AO1 guest observer data. We include in this work two new *XMM-Newton* AO18 observations obtained as part of our semi-annual monitoring program. Because of the increase in the low-energy X-ray opacity of the *Chandra* ACIS window, it is no longer practical to use that instrument given the soft X-ray spectrum of 1E 1207.4–5209.

Table 1 presents a complete log of timing observations for 1E 1207.4–5209. Previously published *Chandra* and *XMM-Newton* data sets used herein are fully described in our earlier work (Gotthelf & Halpern 2007; Halpern & Gotthelf 2011; Gotthelf et al. 2013; Halpern & Gotthelf 2015). Below we detail the preparation of the *NICER* data sets, included for the first time in our analysis of the pulsar. All data sets were reprocessed and reduced using the latest software for each mission. Photon arrival times were converted to barycentric dynamical time (TDB) using the DE405 solar system ephemeris and the *Chandra* coordinates given in Gotthelf et al. (2013), shown in Table 2. Significant proper motion has not been detected (Halpern & Gotthelf 2015). In this analysis we include only photons that fall in the 0.5–1.6 keV energy range, optimal for the pulsar’s observed spectrum. For the *XMM-Newton* and the *Chandra* data sets, we extracted photons using 30'' and 1''8 radius circular apertures, respectively.

The Neutron Star Interior Composition Explorer (*NICER*; Gendreau & Arzoumanian 2017) is an X-ray telescope attached to the International Space Station that provides sub microsecond time resolution in the 0.2–12 keV band. The *NICER* telescope consists of a set of 52 operational non-imaging silicon drift detectors (Prigozhin et al. 2016), each at the focus of an X-ray concentrator (Okajima et al. 2016) that subtends a 4' radius field-of-view. The nominal effective area of the telescope is 1900 cm² at 1.5 keV.

The *NICER* data sets were reduced and analyzed using the NICERDAD software suite distributed in the FTOOLS package, version 24Jun2019_V6.26.1, and the most up-to-date calibration files. We generated cleaned event files using the `nicer12` script that applied the standard filtering criteria. The data were further reduced by excluding detectors with anomalous count rates > 5 sigma above the mean rate, computed using all available detectors, in the energy range of interest. Similarly, we iteratively excluded time intervals with high background rates by comparing the event rate in 10 s steps to the mean rate.

Since its launch in 2017, *NICER* has observed 1E 1207.4–5209 a total of 148 times to-date. Each observation is defined by a unique ObsID number and typically comprises short exposures (50% are less than 1.2 ks) spread over multiple satellite orbits, and often containing multi-day gaps within, and between. These exposures are generally too short to generate a precise pulse phase measurement needed for our timing analysis. However, by concatenating adjacent observations we obtained eight sufficiently compact *NICER* data sets that contained the minimum number of events required to measure an independent pulse phase, as described below.

3. TIMING ANALYSIS

TABLE 1
LOG OF X-RAY TIMING OBSERVATIONS OF 1E 1207.4–5209

Mission	Instrument /Mode	ObsID	Date (UT)	Expo ^a (ks)
<i>Chandra</i>	ACIS-S3/CC	751	2000 Jan 06	32.4
<i>XMM</i>	EPIC-pn/sw	0113050501	2001 Dec 23	27.0
<i>Chandra</i>	ACIS-S/CC	2799	2002 Jan 05	30.3
<i>XMM</i>	EPIC-pn/sw	0155960301	2002 Aug 04	128.0
<i>XMM</i>	EPIC-pn/sw	0155960501	2002 Aug 06	129.0
<i>Chandra</i>	ACIS-S/CC	3915	2003 Jun 10	155.1
<i>Chandra</i>	ACIS-S/CC	4398	2003 Jun 18	114.7
<i>XMM</i>	EPIC-pn/sw	0304531501	2005 Jun 22	15.1
<i>XMM</i>	EPIC-pn/sw	0304531601	2005 Jul 05	18.2
<i>XMM</i>	EPIC-pn/sw	0304531701	2005 Jul 10	20.5
<i>XMM</i>	EPIC-pn/sw	0304531801	2005 Jul 11	63.4
<i>XMM</i>	EPIC-pn/sw	0304531901	2005 Jul 12	14.5
<i>XMM</i>	EPIC-pn/sw	0304532001	2005 Jul 17	16.5
<i>XMM</i>	EPIC-pn/sw	0304532101	2005 Jul 31	17.7
<i>XMM</i>	EPIC-pn/sw	0552810301	2008 Jul 02	31.4
<i>XMM</i>	EPIC-pn/sw	0552810401	2008 Dec 22	30.4
<i>Chandra</i>	ACIS-S3/CC	14199	2011 Nov 25	31.0
<i>Chandra</i>	ACIS-S3/CC	14202	2012 Apr 10	33.0
<i>XMM</i>	EPIC-pn/sw	0679590101	2012 Jun 22	26.5
<i>XMM</i>	EPIC-pn/sw	0679590201	2012 Jun 24	22.3
<i>XMM</i>	EPIC-pn/sw	0679590301	2012 Jun 28	24.9
<i>XMM</i>	EPIC-pn/sw	0679590401	2012 Jul 02	24.5
<i>XMM</i>	EPIC-pn/sw	0679590501	2012 Jul 18	27.3
<i>XMM</i>	EPIC-pn/sw	0679590601	2012 Aug 11	27.3
<i>Chandra</i>	ACIS-S3/CC	14200	2012 Dec 01	31.1
<i>Chandra</i>	ACIS-S3/CC	14203	2013 May 19	33.0
<i>Chandra</i>	ACIS-S3/CC	14201	2013 Dec 04	33.0
<i>Chandra</i>	ACIS-S3/CC	14204	2014 Jun 20	33.0
<i>XMM</i>	EPIC-pn/sw	0780000201	2016 Jul 28	32.5
<i>XMM</i>	EPIC-pn/sw	0800960201	2017 Jun 22	33.3
<i>XMM</i>	EPIC-pn/sw	0800960301	2017 Jun 23	20.7
<i>XMM</i>	EPIC-pn/sw	0800960401	2017 Jun 24	22.6
<i>XMM</i>	EPIC-pn/sw	0800960501	2017 Jul 03	23.5
<i>NICER</i> ^b	XTI	1020270102	2017 Jul 24	6.1
<i>NICER</i> ^b	XTI	1020270106	2017 Jul 28	14.3
<i>NICER</i> ^b	XTI	1020270110	2017 Aug 01	12.1
<i>XMM</i>	EPIC-pn/sw	0800960601	2017 Aug 10	19.8
<i>Chandra</i>	ACIS-S3/CC	19612	2017 Oct 10	32.9
<i>NICER</i> ^b	XTI	1020270130	2017 Nov 15	20.6
<i>XMM</i>	EPIC-pn/sw	0800960701	2017 Dec 24	19.8
<i>XMM</i>	EPIC-pn/sw	0821940201	2018 Jun 22	33.2
<i>Chandra</i>	ACIS-S3/CC	19613	2018 Aug 27	66.3
<i>NICER</i> ^b	XTI	1020270153-58	2018 Nov 30	7.6
<i>XMM</i> ^b	EPIC-pn/sw	0821940301	2018 Dec 28	26.6
<i>NICER</i> ^b	XTI	2506010101-02	2019 Apr 04	22.3
<i>XMM</i> ^b	EPIC-pn/sw	0842280301	2019 Jul 09	30.8
<i>NICER</i> ^b	XTI	2506010201-02	2019 Jul 19	21.4
<i>NICER</i> ^b	XTI	2506010205-13	2019 Jul 26	6.7

^a Exposure times for *XMM-Newton* EPIC-pn does not reflect the 29% deadtime in the SmallWindow (sw) mode.

^b Newly reported observations. The *NICER* data set are denoted by the ObsID and date of the first of the concatenated set of observations (see Section 2 for details).

For each reprocessed, cleaned event file, we folded the extracted photon arrival times on the pulsar frequency to compute the time-of-arrival (ToA) of phase zero of the pulse. To attempt a phase-connected timing solution, we fit the set of ToAs using the TEMPO software (Hobbs et al. 2006) to a model for the rotation phase of the pulsar including one or two of its frequency derivatives,

$$\phi(t) = \phi_o + f(t - t_o) + \frac{1}{2}\dot{f}(t - t_o)^2 + \frac{1}{6}\ddot{f}(t - t_o)^3.$$

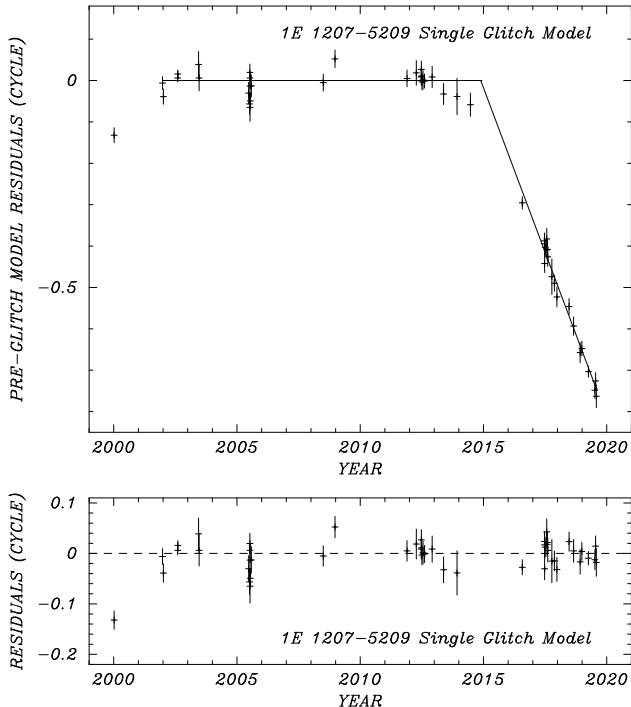


FIG. 1.— Top: Pulse-phase residuals from the revised pre-glitch timing solution (Table 2) for the single glitch model of Gotthelf & Halpern (2018). A glitch epoch of 2014 November 21 is estimated from the intersection of the pre- and post-glitch fits (solid lines). The year 2000 *Chandra* data point is not included in the fit (see Section 3.1 for details). Bottom: Combined residuals from the pre- and post-glitch timing models. The overall $\chi^2_\nu = 1.44$ for 42 degrees of freedom (DoF), taking into account the fit parameters for each interval.

Initially, we obtained the fold frequency from a periodogram search for the maximum power around the expected frequency, determined from the ephemeris of Gotthelf & Halpern (2018). After fitting these ToAs to generate an intermediate timing solution, we iterated a refined set of ToAs by folding the arrival times on the frequencies predicted by this solution, before and after the glitch.

The summed pulse profile, generated by folding all the data together, is found to be well-characterized by a sine function. We use this model to determine the phase zero for the ToAs, most accurately computed from the unbinned photon arrival times, t_i , from the ratio of the Fourier sums,

$$\psi_{\text{sine}} = \tan^{-1} \left\{ \frac{\sum \sin[2\pi\phi(t_i)]}{\sum \cos[2\pi\phi(t_i)]} \right\}.$$

The uncertainty in the phase is determined from a least-squares fit of a sine function to the pulse profile folded in 20 phase bins. In this work, phase zero is defined as the minimum of the modeled sine.

3.1. Single Glitch Fit

Figure 1 graphs the ToA phase residuals from the pre-glitch timing solution given in Table 2, obtained using data points from 2002–2015. After 2015, a linear deviation from this solution is evident and its slope gives a change of frequency of $\Delta f = (5.03 \pm 0.16) \times 10^{-9}$ Hz and a glitch magnitude of $\Delta f/f_{\text{pred}} = (2.134 \pm 0.066) \times 10^{-9}$. The predicted frequency f_{pred} is found by extrapolat-

TABLE 2
SINGLE GLITCH EPHEMERIDES FOR 1E 1207.4–5209

Parameter	Value ^a
R.A. (J2000)	12 ^h 10 ^m 00 ^s .91
Decl. (J2000)	−52°26′28″.4
Surface dipole field, B_s	9.8×10^{10} G
Spin-down luminosity, \dot{E}	1.1×10^{31} erg s ^{−1}
Characteristic age, $\tau_c \equiv P/2\dot{P}$	303 Myr
Pre-glitch Timing Solution (2002–2014)	
Epoch of ephemeris (MJD TDB)	54547.00000198
Span of ephemeris (MJD)	52266–56829
Frequency, f	$2.357763492491(28)$ s ^{−1}
Frequency derivative, \dot{f}	$-1.2317(66) \times 10^{-16}$ s ^{−2}
Period, P	0.4241307506816(50) s
Period derivative, \dot{P}	$2.216(12) \times 10^{-17}$
χ^2_ν [DoF]	1.80[25]
Post-Glitch Timing Solution (2016–2019)	
Epoch of ephemeris (MJD TDB)	58144.00000220
Span of ephemeris (MJD)	57597–58695
Frequency, f	$2.35776345915(16)$ s ^{−1}
Frequency derivative, \dot{f}	$-1.01(12) \times 10^{-16}$ s ^{−2}
Period, P	0.424130756679(30) s
Period derivative, \dot{P}	$1.81(21) \times 10^{-17}$
χ^2_ν [DoF]	0.91[17]
Glitch epoch (MJD) ^b	56982(6)
Δf	$5.03(16) \times 10^{-9}$ s ^{−1}
$\Delta f/f_{\text{pred}}$	$2.134(66) \times 10^{-9}$

Note – Derived parameters (B_s , \dot{E} , τ_c) are based on the pre-glitch timing solution.

^a Uncertainties in the last digits are given in parentheses.

^b Epoch of the glitch estimated by matching the zero phase of the two timing solutions; this assumes a constant post-glitch \dot{f} .

ing the pre-glitch solution to the glitch epoch of 2014 November 21 (MJD 56982), estimated by matching the zero phase of the pre- and post glitch solutions. The linearity of the post-glitch line is consistent with a simple glitch in frequency; there is no evidence of a change in the frequency derivative as suggested in Gotthelf & Halpern (2018). If there is any short-term partial recovery after the glitch, it is not resolved by these sparse data. The magnitude of the glitch is also about half of the value in Gotthelf & Halpern (2018). Nevertheless, this is the same timing solution as the one published previously, in the sense that the cycle count calculated over the data span common to both analyses is the same. The parameters of the revised post-glitch timing solution are simply made more accurate by including the new data. For the entire data set, $\chi^2_\nu = 1.44$ for 42 DoF, taking into account the fit parameters for each interval. We also note that the very first ToA, the *Chandra* observation of 2000, does not seem to fit with the pre-glitch analysis, so we ultimately excluded it from the fits for the pre-glitch ephemeris in Table 2. This data point is nevertheless shown for reference in Figure 1 and in subsequent residual graphs.

3.2. Two Glitch Fit

When extrapolated back to earlier times, the updated post-glitch timing solution is sufficiently well sampled to reveal deviations in the residuals that suggest an earlier glitch likely occurred around epoch 2010. Figure 2

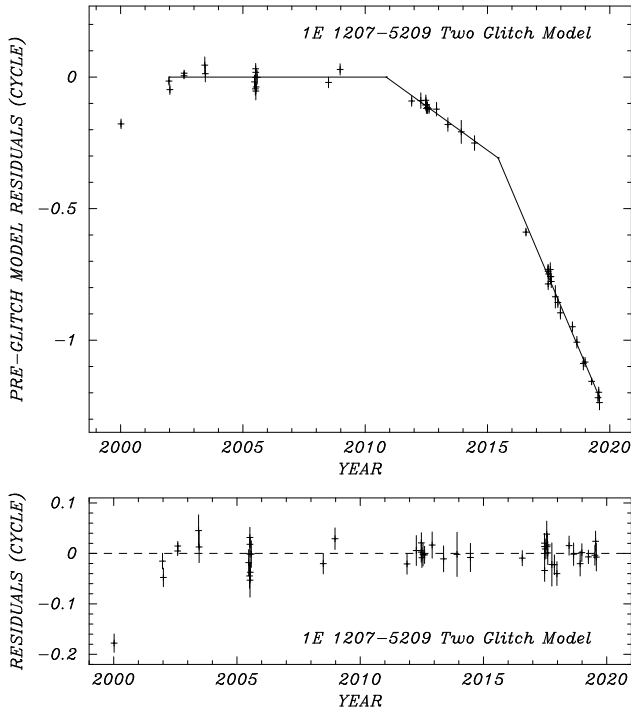


FIG. 2.— Top: Pulse-phase residuals from the pre-glitch timing solution presented in Table 3, modelled as two successive glitch-like changes in frequency. Glitch epochs of 2010 November 09 and 2014 May 23 are estimated from the intersection of the respective pre- and post-glitch fits (solid lines). The year 2000 *Chandra* data point is not included in the fit (see Section 3.2 for details). Bottom: Combined residuals from timing model fits to the three inter-glitch intervals. The overall $\chi^2_\nu = 1.23$ for 39 DoF, taking into account the fit parameters for each interval.

presents the residuals from a 2002–2010 pre-glitch phase-connected solution extrapolated to later times. A clear transition occurred at the estimated epoch 2010 November 9 (MJD 55509) with $\Delta f = (2.13 \pm 0.36) \times 10^{-9}$ Hz and $\Delta f/f_{\text{pred}} = (9 \pm 2) \times 10^{-10}$, about half the value for the single glitch fit. Comparing the residual of the second post-glitch solution to the first post-glitch solution, we now measure a smaller glitch that occurred at 2014 May 23 (MJD 56800), with $\Delta f = (9 \pm 2) \times 10^{-10}$ Hz and $\Delta f/f_{\text{pred}} = (3.70 \pm 0.66) \times 10^{-10}$. Thus, there is now evidence of at least three distinct spin-down intervals whose ephemerides are given in Table 3. The entire data set fitted with this model has $\chi^2_\nu = 1.23$ for 39 degrees DoF, taking into account the fit parameters for each interval.

The timing models presented above are unable to fit the year 2000 data point to within the uncertainty of the ToA. This particular observation is hard to dismiss since it yields a highly significant detection of the pulsed signal, and a high-quality ToA. Furthermore, we have found no evidence for systematic error associated with the data reduction or measurement of the ToA. If there was a glitch between 2000 and 2002, it could explain the discrepant point in 2000. This would suggest that glitches in 1E 1207.4–5209 occur at an interval of 4–10 years.

3.3. Alternative Model Fits

Given the uncertain physics of CCO pulsars in particular and glitches in general, we also tested alternative timing models for the full data set that might fit without

TABLE 3
TWO GLITCH EPHEMERIDES FOR 1E 1207.4–5209

Parameter	Value ^a
Pre-glitch Timing Solution (2002–2008)	
Epoch of ephemeris (MJD TDB)	53544.00000442
Span of ephemeris (MJD)	52266–54822
Frequency, f	$2.357763503102(75) \text{ s}^{-1}$
Frequency derivative, \dot{f}	$-1.278(21) \times 10^{-16} \text{ s}^{-2}$
Period, P	$0.424130748773(14) \text{ s}$
Period derivative, \dot{P}	$2.299(38) \times 10^{-17}$
χ^2_ν [DoF]	2.32[13]
Post-2010 Glitch Timing Solution (2011–2014)	
Epoch of ephemeris (MJD TDB) ^b	56359.00000177
Span of ephemeris (MJD)	55890–56829
Frequency, f	$2.35776347415(36) \text{ s}^{-1}$
Frequency derivative, \dot{f}	$-1.03(27) \times 10^{-16} \text{ s}^{-2}$
Period, P	$0.424130753981(64) \text{ s}$
Period derivative, \dot{P}	$1.85(49) \times 10^{-17}$
χ^2_ν [DoF]	0.26[9]
Glitch epoch (MJD) ^b	55509(36)
Δf	$2.13(36) \times 10^{-9} \text{ s}^{-1}$
$\Delta f/f_{\text{pred}}$	$9(2) \times 10^{-10}$
Post-2015 Glitch Timing Solution (2016–2019)	
Epoch of ephemeris (MJD TDB)	58144.00000219
Span of ephemeris (MJD)	57597–58695
Frequency, f	$2.35776345915(16) \text{ s}^{-1}$
Frequency derivative, \dot{f}	$-1.01(12) \times 10^{-16} \text{ s}^{-2}$
Period, P	$0.424130756679(30) \text{ s}$
Period derivative, \dot{P}	$1.81(21) \times 10^{-17}$
χ^2_ν [DoF]	0.91[17]
Glitch epoch (MJD) ^b	56800(8)
Δf	$9(2) \times 10^{-10} \text{ s}^{-1}$
$\Delta f/f_{\text{pred}}$	$3.70(66) \times 10^{-10}$

^a Uncertainties in the last digits are given in parentheses.

^b Epoch of the glitch estimated by matching the zero phase of the two timing solutions; this assumes a constant post-glitch \dot{f} .

using glitches. In such models there is no particular justification for excluding the 2000 *Chandra* data point, so we include it. The timing solutions for these alternative models are given in Table 4.

Starting with a simple quadratic timing model (with one frequency derivative) leaves a sinusoidal oscillation in the phase residuals. As shown in Figure 3, these residuals can be fully accounted for by a circular binary orbit with a period of 14.77 ± 0.60 yr and a projected semi-major axis of 0.049 ± 0.010 lt-s (Table 4). The fit, with $\chi^2_\nu = 1.13$ for 43 DoF, is as good as or better than the glitch models. We discuss the possible interpretation of these fitted parameters in Section 4.2.

We also consider a cubic polynomial, which includes a frequency second derivative, over the entire span of the observations. This can also fully model the set of ToAs, but only if the 2000 point is excluded (Figure 3, bottom panel). Without the 2000 point, $\chi^2_\nu = 1.34$ for 44 DoF, but including it yields $\chi^2_\nu = 3.04$ for 45 DoF. Parameters from both versions of the cubic fit are given in Table 4. The frequency second derivative \ddot{f} , or the braking index, defined as $n \equiv f\ddot{f}/\dot{f}^2$, are often used to characterize

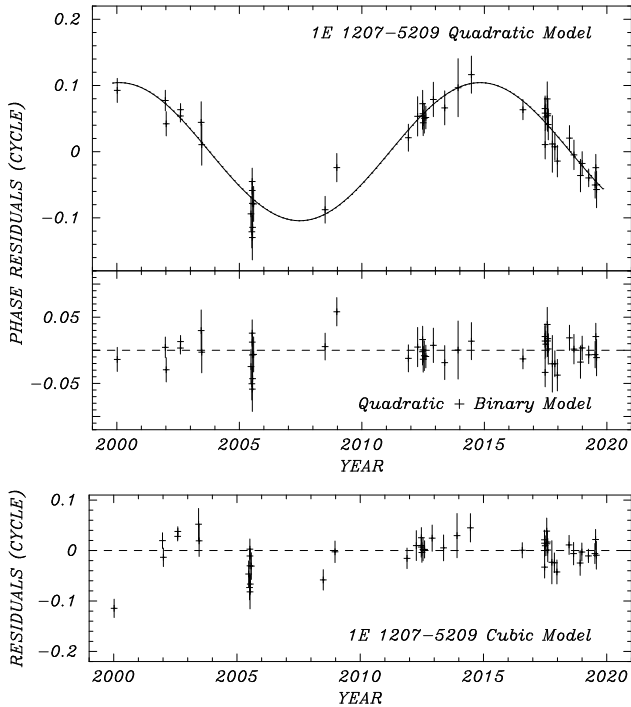


FIG. 3.— Pulse-phase residuals from the alternative timing models presented in Table 4 that do not involve glitch(es). These fits include the 2000 *Chandra* data point (see Section 3.3 for details). Top: A quadratic fit leaves sinusoidal oscillations in the phase residuals (upper panel). The lower panel shows the residuals after a binary orbit having a period of 14.77 ± 0.60 yr and projected semi-major axis of 0.049 ± 0.010 lt-s is added. Bottom: Residuals from a cubic polynomial fit (including frequency second derivative).

timing noise in pulsars. In Section 4.2 we discuss the cubic fit in terms of timing noise.

4. DISCUSSION

4.1. Glitch Models

Taking the glitch timing models at face value, continued observations of 1E 1207.4–5209 show that the previously discovered glitch is better described as two smaller ones separated by 3.5 yr. In addition, there is no longer any evidence for a large change in frequency derivative as suggested by Gotthelf & Halpern (2018). Nevertheless, the mere detection of glitching activity in a pulsar with such a small spin-down rate is unprecedented, as we shall describe below. As shown most recently by Espinoza et al. (2011) and Fuentes et al. (2017), glitch activity is best correlated with \dot{f} , such that $\approx 1\%$ of the long-term spin-down is reversed by glitching. In the context of the vortex creep theory of glitches (Alpar et al. 1984), this implies that 1% or more of the moment of inertia of the NS is contained in a crustal superfluid whose vortices are repeatedly pinned and unpinned.

The glitch activity parameter for an individual pulsar is defined as

$$\dot{f}_g \equiv \frac{\sum_j \Delta f_j}{T},$$

where the numerator is the sum of the changes in frequency over the glitches, and T is the total span of the observations. The linear correlation in which $\dot{f}_g \approx 0.01|\dot{f}|$ only becomes apparent when glitch activity is summed

TABLE 4
ALTERNATIVE TIMING SOLUTIONS FOR 1E 1207.4–5209

Parameter	Value ^a
Quadratic + Binary Timing Solution (2000-2019)	
Epoch of ephemeris (MJD TDB)	55478.00000457
Span of ephemeris (MJD)	51549–58695
Frequency, f	$2.357763483701(46) \text{ s}^{-1}$
Frequency derivative, \dot{f}	$-1.1215(39) \times 10^{-16} \text{ s}^{-2}$
Period, P	$0.4241307522627(84) \text{ s}$
Period derivative, \dot{P}	$2.0176(71) \times 10^{-17}$
Binary period	$14.77(60) \text{ yr}$
Projected semi-major axis	$0.049(10) \text{ lt-s}$
Time of ascending node (MJD)	$55611(57)$
Longitude of periastron passage	$342^\circ \pm 4^\circ$
$\chi^2_{\nu}[\text{DoF}]$	$1.13[43]$
Cubic Timing Solution (2000-2019)	
Epoch of ephemeris (MJD TDB)	55478.00000457
Span of ephemeris (MJD)	51549–58695
Frequency, f	$2.357763483047(42) \text{ s}^{-1}$
Frequency derivative, \dot{f}	$-1.1193(20) \times 10^{-16} \text{ s}^{-2}$
Frequency second derivative, \ddot{f}	$6.57(39) \times 10^{-26} \text{ s}^{-3}$
Period, P	$0.4241307523805(76) \text{ s}$
Period derivative, \dot{P}	$2.0135(36) \times 10^{-17}$
Period second derivative, \ddot{P}	$-1.181(70) \times 10^{-26} \text{ s}^{-1}$
$\chi^2_{\nu}[\text{DoF}]$	$3.04[45]$
Cubic Timing Solution (2002-2019)	
Epoch of ephemeris (MJD TDB)	55478.00000451
Span of ephemeris (MJD)	52266–58695
Frequency, f	$2.357763482808(50) \text{ s}^{-1}$
Frequency derivative, \dot{f}	$-1.1255(21) \times 10^{-16} \text{ s}^{-2}$
Frequency second derivative, \ddot{f}	$9.18(49) \times 10^{-26} \text{ s}^{-3}$
Period, P	$0.4241307524235(90) \text{ s}$
Period derivative, \dot{P}	$2.0246(38) \times 10^{-17}$
Period second derivative, \ddot{P}	$-1.651(88) \times 10^{-26} \text{ s}^{-1}$
$\chi^2_{\nu}[\text{DoF}]$	$1.34[44]$

^a Uncertainties in the last digits are given in parentheses.

over groups of pulsars binned in \dot{f} . However, this linear correlation holds only in the range $10^{-14} < |\dot{f}| < 10^{-11} \text{ s}^{-2}$. In addition, f_g is dominated in this range by the largest glitches, which have $\Delta f/f \sim 10^{-6}$. For smaller values of $|\dot{f}|$, only small glitches occur, and glitch activity plummets such that no pulsar with $|\dot{f}| < 3 \times 10^{-16} \text{ s}^{-2}$ has been observed to glitch in 1780 pulsar years of monitoring (Fuentes et al. 2017). The upper limit on the glitch parameter for such small $|\dot{f}|$ is $\dot{f}_g < 10^{-19} \text{ s}^{-2}$ by extrapolation from pulsars with larger $|\dot{f}|$.

In contradistinction, 1E 1207.4–5209 with its $\dot{f} = -1.2 \times 10^{-16} \text{ s}^{-2}$ has glitched two or three times in 20 years, with a glitch activity parameter of $\dot{f}_g = (5 - 9) \times 10^{-18} \text{ s}^{-2}$, which has the result of reversing $\approx 4 - 7\%$ of its spin-down. Evidently 1E 1207.4–5209 experiences higher glitch activity relative to its spin-down rate than most pulsars, its activity being dominated by small but frequent glitches.

4.2. Alternative Models

Alternative models without glitches are equally good in fitting the timing data on 1E 1207.4–5209. In particular, the fit of quadratic spin-down plus binary orbit has the

lowest χ^2 of the all of the models tested here. If the sinusoidal component is due to an orbital motion, the minimum mass of the companion would be $6.8 M_{\oplus}$ for a $1.4 M_{\odot}$ NS, which is similar to the original pulsar planets PSR B1257+12 B and C (Konacki & Wolszczan 2003), albeit with a much longer period of ≈ 15 yr instead of 2–3 months. But the fitted period, only slightly shorter than the time span of the observations, is a typical result of red noise, a known characteristic of the timing noise of pulsars, and thus a more likely interpretation. In the following, we quantify the timing noise and compare it with trends in the general pulsar population.

Several diagnostics of timing noise have been introduced over the years. They were reviewed recently by Namkham et al. (2019) in their study of timing noise in 129 middle-aged pulsars, and we employ three of the methods here. First is a simple metric favored by Shannon & Cordes (2010),

$$\sigma_{\text{TN},2}^2 = \sigma_{\text{R},2}^2 - \sigma_{\text{W}}^2,$$

where $\sigma_{\text{R},2}$ is the root-mean-square (rms) of the measured residuals from a second-order polynomial fit, and σ_{W} is the typical uncertainty of a ToA. (The subscripts R and W refer to red and white noise processes, respectively.) Shannon & Cordes (2010) found for hundreds of canonical pulsars (not millisecond pulsars or magnetars) that the mean value of $\sigma_{\text{TN},2}$ scales with the spin parameters as

$$\bar{\sigma}_{\text{TN},2} = C_2 f^{\alpha} |\dot{f}|^{\beta} T^{\gamma} \mu\text{s},$$

where $C_2 = 41.7$, $\alpha = -0.9$, $\beta = 1.00$, and $\gamma = 1.9$. Recognizing that there is large scatter in $\sigma_{\text{TN},2}$, Shannon & Cordes (2010) modelled the distribution as log-normal, and found that the standard deviation of $\log(\sigma_{\text{TN},2})$ is $\delta = 1.6$

This method is applicable to the quadratic fit of Figure 3 (top). The rms timing residual is $\sigma_{\text{R},2} = 27.3$ ms, while the average uncertainty of a ToA is $\sigma_{\text{W}} = 9.5$ ms; therefore, $\sigma_{\text{TN},2} = 25.6$ ms. In comparison, the fitted value of $\bar{\sigma}_{\text{TN},2}$ from Shannon & Cordes (2010) corresponding to the timing parameters of 1E 1207.4–5209 is $\approx 100 \mu\text{s}$ (see also the data in Figure 6 of Namkham et al. 2019). The observed residuals therefore exceed the pulsar average by a factor of ≈ 250 , which is much greater than the scatter of $10^{1.6}$ found by Shannon & Cordes (2010) and the scatter of the data points in Namkham et al. (2019). This shows that, if the timing irregularities in 1E 1207.4–5209 are timing noise, it is behaving like a pulsar with 2–3 orders of magnitude larger $|\dot{f}|$ or B_s .

An earlier parameterization of timing noise is that of Arzoumanian et al. (1994), who used the frequency second derivative measured over a time span of $T = 10^8$ s to define

$$\Delta_8 = \log \left(\frac{1}{6f} |\ddot{f}| T^3 \right).$$

Arzoumanian et al. (1994), Hobbs et al. (2010), and Namkham et al. (2019) showed that Δ_8 is positively correlated with \dot{f} . Unfortunately, this and other metrics are sensitive to the time span of the observation, since \ddot{f} itself, being the result of red noise, generally increases with T . Therefore, Δ_8 should not be used to compare pulsars over different time spans. But since the ToAs

of 1E 1207.4–5209 are not nearly as precise as those of radio pulsars, we cannot even get a significant measurement of \ddot{f} if we reduce the time span of the fit to 10^8 s. Acknowledging the limitations of such a comparison, we nevertheless calculate $\Delta_8 = 0.04$ from either version of the cubic fit in Table 4, finding that it is 2–3 orders of magnitude larger than that of pulsars with similar \dot{f} , and at the high end of all pulsars. This rather extreme discrepancy argues that 1E 1207.4–5209 is much noisier than pulsars with similar spin-down rates.

Finally, the braking index itself can be used to characterize timing noise. For the timing parameters of the two cubic fits in Table 4, $n = 1.2 \times 10^7$ or 1.7×10^7 , which are off the scale of values plotted in Namkham et al. (2019). Pulsars of similar \dot{f} or B_s have $n < 2 \times 10^6$.

5. CONCLUSIONS

Whether the timing irregularities of 1E 1207.4–5209 are described as two or three glitches, or as timing noise, the magnitude of the effects are much greater than in radio pulsars of similar spin-down rate or dipole magnetic field strength. Because 1E 1207.4–5209 displays no evidence of magnetospheric activity, while its timing properties are commensurate with those of the young pulsar population, an internal property such as high temperature or high B -field strength is implicated. Ho (2015) proposed that glitches could be triggered by the motion of magnetic fields through the NS crust, interacting with the neutron superfluid there. If so, a magnetic field much stronger than the surface dipole field is buried in the crust of 1E 1207.4–5209. Ho (2015) was envisioning large glitches like those of the Vela pulsar, whereas only small glitches have so far been detected from 1E 1207.4–5209, which distinguishes it from the more energetic pulsars.

Timing noise has been attributed to variability in the interaction of the crustal superfluid with the Coulomb lattice of the solid crust (Jones 1990), turbulence of the superfluid (Melatos & Link 2014), or fluctuations in the structure of the magnetosphere, e.g., state switching (Lyne et al. 2010). Just as for glitches, internal effects would be favored as the cause of timing noise in 1E 1207.4–5209 because of its lack of magnetospheric activity.

Finally, as discussed in Gotthelf & Halpern (2018), it has not been ruled out that low-level accretion from an undetected fall-back debris disk could be the cause of its timing fluctuations while making a negligible contribution to the luminosity of 1E 1207.4–5209. The present results do not alter those arguments about accretion torques, and we do not repeat them here, except to recall the possible connection between field burial and formation of a residual disk, which would require only a small fraction of the fall-back debris to be held in reserve for long-term accretion from a disk.

Support for this work was provided by NASA through *XMM* grants 80NSSC18K0452, 80NSSC19K0866, *NICER* grant 80NSSC19K1461, and *Chandra* Award SAO GO7-18063X issued by the *Chandra* X-ray Observatory Center, which is operated by the Smithsonian Astrophysical Observatory for and on behalf of NASA under contract NAS8-03060. This investigation is based

partly on observations obtained with *XMM-Newton*, an ESA science mission with instruments and contributions directly funded by ESA Member States and NASA. This

research has made use of data and/or software provided by the High Energy Astrophysics Science Archive Research Center (HEASARC), which is a service of the Astrophysics Science Division at NASA/GSFC.

REFERENCES

- Alpar, M. A., Pines, D., Anderson, P. W., & Shaham, J. 1984, *ApJ*, 276, 325
- Arzoumanian, Z., Nice, D. J., Taylor, J. H., & Thorsett, S. E. 1994, *ApJ*, 422, 671
- Bignami, G. F., Caraveo, P. A., De Luca, A., & Mereghetti, S. 2003, *Natur*, 423, 725
- De Luca, A., Mereghetti, S., Caraveo, P. A., et al. 2004, *A&A*, 418, 625
- De Luca, A. 2017, *JPhCS*, 932, 012006
- Espinoza, C. M., Lyne, A. G., Stappers, B. W., & Kramer, M. 2011, *MNRAS*, 414, 1679
- Fuentes, J. R., Espinoza, C. M., Reisenegger, A., et al. 2017, *A&A*, 608, A131
- Gendreau, K., & Arzoumanian, Z. 2017, *NatAs*, 1, 895
- Gotthelf, E. V., & Halpern, J. P. 2007, *ApJL*, 664, L35
- Gotthelf, E. V., & Halpern, J. P. 2018, *ApJ*, 866, 154
- Gotthelf, E. V., Halpern, J. P., Alford, J. 2013, *ApJ*, 765, 58
- Halpern, J. P., & Gotthelf, E. V. 2010, *ApJ*, 709, 436
- Halpern, J. P., & Gotthelf, E. V. 2011, *ApJL*, 733, L28
- Halpern, J. P., & Gotthelf, E. V. 2015, *ApJ*, 812, 61
- Ho, W. C. G. 2015, *MNRAS*, 452, 845
- Hobbs, G. B., Edwards, R. T., & Manchester, R. N. 2006, *MNRAS*, 369, 655
- Hobbs, G., Lyne, A. G., & Kramer, M. 2010, *MNRAS*, 402, 1027
- Jones, P. B. 1990, *MNRAS*, 246, 364
- Konacki, M. & Wolszczan, A. 2003, *ApJL*, 591, L47
- Lyne, A., Hobbs, G., Kramer, M., Stairs, I., & Stappers, B. 2010, *Sci*, 329, 408
- Melatos, A., & Link, B. 2014, *MNRAS*, 437, 21
- Mereghetti, S., De Luca, A., Caraveo, P. A., et al. 2002, *ApJ*, 581, 1280
- Namkham, N., Jaroenjittichai, P., & Johnston, S. 2019, *MNRAS*, 487, 5854
- Okajima, T., Soong, Y., Balsamo, E. R., et al. 2016, *Proc. SPIE*, 9905, 99054X
- Pavlov, G. G., Sanwal, D., Garmire, G. P., & Zavlin, V. E. 2002, in *ASP Conf. Ser. 271, Neutron Stars in Supernova Remnants*, ed. P. O. Slane & B. M. Gaensler (San Francisco, CA: ASP), 247
- Prigozhin, G., Gendreau, K., Doty, J. P., et al. 2016, *Proc. SPIE*, 9905, 99051I
- Sanwal, D., Pavlov, G. G., Zavlin, V. E., & Teter, M. A. 2002, *ApJL*, 574, L61
- Shannon, R. M., & Cordes, J. M. 2010, *ApJ*, 725, 1607
- Zavlin, V. E., Pavlov, G. G., Sanwal, D., & Trümper, J. 2000, *ApJL*, 540, L25